論文 / 著書情報
Article / Book Information

Title	Upconversion Properties of Y2O3:Er,Yb Nanoparticles Prepared by Laser Ablation in Water
Authors	Yuji Onodera, Takashi Nunokawa, Osamu Odawara, Hiroyuki Wada
Citation	Journal of Luminescence, Vol. 137, , p. 220
Pub. date	2013, 1
DOI	http://dx.doi.org/10.1016/j.jlumin.2012.12.033
Creative Commons	See next page.

Title:

Upconversion Properties of Y_2O_3:Er,Yb Nanoparticles Prepared by Laser Ablation in Water

Authors:

Yuji Onodera, Takashi Nunokawa, Osamu Odawara and Hiroyuki Wada

Affiliation:

Tokyo Institute of Technology, 4259 Nagatsuta, Midori-ku, Yokohama 226-8502 Japan

Corresponding author:

Hiroyuki Wada (Prof. Ph.D.)

E-mail: wada.h.ac@m.titech.ac.jp

Postal address: 4259 Nagatsuta, #J2-41, Midori-ku, Yokohama 226-8502 Japan

Phone/Fax: +81 45 924 5362

Keywords:

Nanoparticle; Laser ablation; Upconversion

Doi:10.1016/j.jlumin.2012.12.033

Abstract:

Y_2O_3:Er,Yb nanoparticles were successfully prepared by laser ablation in liquid, and their upconversion properties were investigated. The particles were prepared by irradiating a Y_2O_3:Er,Yb target in water with a 532-nm pulsed laser beam. The prepared nanoparticles were determined to be composed of Y_2O_3, without any by-products, by X-ray diffraction. The average particle size of the nanoparticles measured by electron microscopy was a few tens of nanometers, which depended on the energy density of the irradiating laser beam. Upconversion luminescence of the nanoparticles was observed by the excitation of the laser diode at a wavelength of 980 nm. An increase by 33 % in the ratio of red emission ($^4F_{9/2} \rightarrow {}^4I_{15/2}$) to green emission ($^2H_{11/2}/^4S_{3/2} \rightarrow {}^4I_{15/2}$) was observed with a decrease in the size of the nanoparticles from 21.5 nm to 11.1 nm. This high ratio is useful for biomedical applications because of the high transparency of this wavelength in the human body. The number of photons generated by the upconversion luminescence of the nanoparticles was investigated. The number of photons involved in the process of the nanoparticles was three, which was attributed to nonradiative relaxation due to the large specific surface area of the particles; in contrast, the normal number of photons involved in the process of Y_2O_3:Er,Yb bulk is two.

Doi:10.1016/j.jlumin.2012.12.033

1. Introduction

Upconversion is one of the most interesting optical properties. Through upconversion, high-energy photons are generated by the absorption of lower-energy photons. Upconversion materials emit visible light by the irradiation of long-wavelength, e.g., near-infrared (IR) light, while visible emission is observed by the excitation of shorter-wavelength light, such as ultraviolet (UV) light in the case of normal fluorescence. These phenomena, which are basically multiphoton processes, have been extensively investigated by many researchers.[1-5] The number of photons related to the luminescence is equal to the slope of the double logarithmic plot of excitation and emission intensity.[6] The typical activator of upconversion is the erbium (Er) ion, which has various energy levels due to its 4*f* electrons and emits green and red light.[7] The ytterbium (Yb) ion, which shows IR absorption at approximately 980 nm due to an $^5F_{5/2} \rightarrow {}^5F_{7/2}$ transition, plays an important role as a sensitizer, increasing the upconversion intensity by energy transfer.[1] Fluorides such as $NaYF_4$, YF_3 and $LiYF_4$ have been studied as matrices for upconversion phosphors in recent years.[8] Yttrium oxide (Y_2O_3) is also known to be a stable matrix for upconversion phosphors.[9] One of the promising applications of upconversion materials is solar cell energy conversion of IR light.[10] Normal solar cell is infrared-transparent and does not generate electricity by IR light. However, solar cell with upconversion material generates electricity by IR light, which increases the conversion efficiency of solar cell. The

Doi:10.1016/j.jlumin.2012.12.033

fabrication of upconversion nanoparticles expands the range of possible applications in various fields, for instance, in biomedical applications such as bioimaging and photodynamic therapy.[11-25] In this application, the most important property that is related to upconversion is the absorption of light by living cells, which defines what is called the optical window.[26] The absorption of light by hemoglobin is high at wavelengths less than 600 nm, while the absorption of light by water is high at wavelengths greater than 1400 nm. Both hemoglobin and water are important substances found in large amounts throughout the human body. Therefore, using an upconversion nanoparticle as a marker, highly transparent imaging would be possible and autofluorescence would be reduced to produce high-contrast images. The other advantage is the reduction of thermal damage to living cells.

There are various methods used to prepare nanoparticles that are useful in various fields due to their unique properties. The most widely used method is performed by chemical reactions in the liquid phase.[27] Gas-phase methods are also utilized.[28,29] Pulse laser ablation in the liquid phase produces nanoparticle-dispersed solutions.[30-32] Ablation is the phenomenon in which chemical species such as neutral atoms, molecules, ions, radicals, clusters and electrons are emitted from the surface of a target material irradiated by a focused laser beam with an energy density above a certain threshold. This method is typically applied to metal materials.[30-32] Some researchers have used this method to prepare inorganic nanoparticles except metal.[33-43] This

Doi:10.1016/j.jlumin.2012.12.033

method can be applied to optical materials such as phosphors.[44-46] Moreover, this method has various advantages. 1) Nanoparticle-dispersed solutions with high bioaffinity can be easily produced. 2) Pure nanoparticle-dispersed solutions without unreacted starting materials can be obtained. In the case of the chemical-reaction method, the unreacted starting materials remain in the nanoparticle-dispersed solution, causing harmful effects such as cell death to occur. 3) Multielement composite nanoparticles can be prepared. Usually, phosphor materials include multiple elements because of the doping of activators and sensitizers. It is difficult to synthesize these nanoparticles in solution by the chemical-reaction method. 4) Nanoparticles are collected with high efficiency because all generated nanoparticles are trapped by the solvent.

In this study, upconversion nanoparticles were prepared by laser ablation in liquid, and optical investigations of upconversion properties, spectral analyses and the number of photons involved in the process were conducted. We focused on Y_2O_3:Er,Yb because of its high chemical and thermal stability and low toxicity. However, sintering, which promotes the joining of particles by heating, is needed to obtain Y_2O_3:Er,Yb particles.[47-52] Therefore, it is generally difficult to obtain Y_2O_3:Er,Yb nanoparticle-dispersed solutions. Nevertheless, we successfully prepared a Y_2O_3:Er,Yb nanoparticle-dispersed solution by laser ablation in liquid. The other problem we faced was the emission wavelength of Y_2O_3:Er,Yb particles. The main emission band of Y_2O_3:Er,Yb particles is usually green, to which a living body is opaque. We increased

Doi:10.1016/j.jlumin.2012.12.033

the particles' ratio of red to green emission by reducing the particle size.

2. Experimental

Y_2O_3:Er,Yb upconversion nanoparticles were prepared by laser ablation in liquid which was similar to previous works.[46,53] The upconversion properties of the fine nanoparticles were investigated in this study. The laser ablation target was synthesized by the co-precipitation method. Yttrium nitrate hexahydrate (Kanto Chemical), erbium nitrate pentahydrate (Mitsuwa Chemicals), ytterbium nitrate hydrate (Wako Pure Chemical Industries) and ammonia water (Kanto Chemical, 28.0-30.0%) were used without further purification. Yttrium nitrate (1.1 mmol) and erbium nitrate (11.4 mmol) were dissolved in DI water (50 ml) for 30 minutes under ultrasonication and stirred for 1 hour. Ammonia water (11 ml) was added to the solution, which was then stirred for 2 hours. After 24 hours of aging, the precipitate was washed and dried at 60°C for 12 hours. The prepared precursor $Y(OH)_3$: Er,Yb was sintered in an electric furnace at 900°C for 2 hours to synthesize Y_2O_3:Er,Yb. These particles were pressed at room temperature under a pressure of 200 MPa for 6 minutes to obtain a pellet. The pellet was sintered at 1250°C for 4 hours in air to fabricate the laser ablation target.

The target was irradiated in DI water (3 ml) with a focused pulse laser beam. The parameters of the laser (Spectron Laser Systems, SL8585G, Q-switched Nd:YAG laser/SHG)

Doi:10.1016/j.jlumin.2012.12.033

were as follows: the wavelength was 532 nm, the repetition rate was 10 Hz, and the pulse duration was 13 ns. The focal length of the lens was 80 mm. The irradiation time was 5 minutes. The irradiated area on the target was 0.30 mm^2. The energy of the laser was varied by a neutral density (ND) filter from 1.6 to 15.6 mJ/pulse.

The target and nanoparticles were identified using an X-ray diffractometer (XRD, Philips, X'Pert-Pro-MRD). The X-ray radiation of the $CuK_{\alpha 1}$ and $CuK_{\alpha 2}$ lines, whose intensity ratio was $K_{\alpha 2}/K_{\alpha 1}$ = 0.500, was used. The particle size and dispersibility were investigated by scanning electron microscopy (SEM, Hitachi High-Technologies, S-4800). For this observation, the supernatant of the nanoparticle-dispersed solution was dropped onto a carbon membrane on a copper grid, and the solvent was removed by drying in a vacuum oven. The upconversion spectra of the nanoparticles were obtained using a fluorescence spectrophotometer (Hitachi High-Technologies Co. F-7000) at room temperature. A laser diode (ThorLabs, L980P300J, wavelength: 980 nm, maximum power: 300 mW) on an LD mount (TCLDM9) with an electric current-temperature controller (LTC100-B) was used for excitation. For this measurement, the supernatant of the nanoparticle-dispersed solution was dropped onto a glass slide and dried.

3. Results and discussion

The prepared nanoparticles were identified by XRD. Figure 1 shows the XRD pattern of

Doi:10.1016/j.jlumin.2012.12.033

the target (a) and nanoparticles (b). All of the peaks in Figure 1 correspond to those of Y_2O_3. PDF-4+ (ICDD) number of Y_2O_3 is 04-008-6362 and its space group is Ia-3 (206). The crystal structure of Y_2O_3 is cubic and rare earth ions occupy the two Y^{3+} sites of C_2 and S_6 symmetry, which have no inversion symmetry.[54,55] The formation of by-products was not observed in this case, although by-products were sometimes observed to have formed by laser ablation in liquid in previous studies, which indicated a reaction between the target and solvent.[46] In this study, Y_2O_3 was successfully prepared because the melting temperature of the target was high. In our previous studies, by-product was not synthesized and it was found that the formation mechanism of the nanoparticles was fragmentation of target.[53] Therefore, the concentration of Er^{3+} and Yb^{3+} of nanoparticles, which were same as that of target, would be 1 % and 10 %, respectively.

The size of the prepared nanoparticles was investigated by SEM. For reference, an SEM image at 1.6 mJ/pulse is shown in Figure 2. These nanoparticles were well dispersed in the solvent, making them useful for biomedical applications. The particles were not completely spherical, which implies that the particles were formed by the fragmentation of the target. The size distribution of the nanoparticles was determined and is illustrated in Figure 3. Particles with an average size of 11 nm were fabricated under the aforementioned experimental conditions, making them suitable for applications in various research fields. These results are summarized

Doi:10.1016/j.jlumin.2012.12.033

in Figure 4, which plots the average particle size as a function of the irradiating laser energy at the target. These results indicate that the size of the upconversion nanoparticles was slightly controlled by the laser energy.

The upconversion spectra of the prepared nanoparticles at each particle size are shown in Figure 5. The nanoparticles were excited by a laser diode (CW, 980 nm, 220 mW). The fluorescence intensity was normalized to green emission to compare the red and green emission. The ratio of red to green emission increased with decreasing particle size. The efficiency of red emission would be greater than that of green one. Figure 6 shows the energy diagram of the Er^{3+} ion. The upconversion luminescence process occurs as follows.

Green emission is observed after two-step excitations.

$^4I_{15/2} \rightarrow {}^4I_{11/2}$

$^4I_{11/2} \rightarrow {}^2H_{11/2}/{}^4S_{3/2}$

$^2H_{11/2}/{}^4S_{3/2} \rightarrow {}^4I_{15/2}$

Red emission is closely related to a nonradiative relaxation.

$^4I_{15/2} \rightarrow {}^4I_{11/2}$

$^4I_{11/2} \rightarrow {}^4I_{13/2}$ (nonradiative relaxation)

$^4I_{13/2} \rightarrow {}^4F_{9/2}$

$^4F_{9/2} \rightarrow {}^4I_{15/2}$

Doi:10.1016/j.jlumin.2012.12.033

or

$^4I_{15/2} \rightarrow {}^4I_{11/2}$

$^4I_{11/2} \rightarrow {}^2H_{11/2}/{}^4S_{3/2}$

$^2H_{11/2}/{}^4S_{3/2} \rightarrow {}^4F_{9/2}$ (nonradiative relaxation)

$^4F_{9/2} \rightarrow {}^4I_{15/2}$

The second excitation ($^4I_{11/2} \rightarrow {}^2H_{11/2}/{}^4S_{3/2}$, $^4I_{13/2} \rightarrow {}^4F_{9/2}$) in Figures 6 can occur by energy transfer from an excited Yb^{3+} ion.[1] The nonradiative relaxation prevents red emission. In general, nonradiative relaxation is accelerated by the energy transfer through the vibration of molecules such as water. The transition probability per unit time W_{AB} is given by[56,57]

$$W_{AB} = (2\pi\rho_E / h)J^2F \qquad \text{eq. 1}$$

where ρ_E is the state density, h is Planck's constant, J is the coupling constant between the electronic wavefunctions due to nuclear motion and F is the Franck-Condon factor. The transition probability is proportional to the Franck-Condon factor. The Franck-Condon factor decreases significantly with the increase in the vibrational quantum number ν.[57] In other words, the energy transfer to a molecule that has high vibrational energy is likely to occur, which is similar to there being a high probability of thermal relaxation through the high phonon energy of a crystal.[58] The water molecule has high vibrational energy (approximately 3400-3600 cm^{-1})[59-61] compared with other

Doi:10.1016/j.jlumin.2012.12.033

organic solvents, while the energy of nonradiative relaxation associated with red emission is at approximately 3600 cm^{-1}.[7] In this case, the vibrational quantum number of the energy transfer from an excited state to the vibrational energy state of a water molecule is almost one, which indicates a very high probability. Because the solvent used in the laser ablation process was water, water molecules were likely adsorbed to the surface of the nanoparticles. As particles decrease in size, their specific surface area is significantly increased. Thus, the probability of the nonradiative relaxation of the nanoparticles was increased because of their large specific surface area. Moreover, an increase in nonradiative relaxation would enhance the red emission of nanoparticles. The similar phenomena were observed previously.[62] At the same time, however, defects exist on the surface of particles. Because these surface defects also enhance the nonradiative relaxation, the red emission of nanoparticles is stronger than the green emission.

The relation between excitation and emission intensity is given by[1,6]

$$P_{em} = AP_{ex}^{n} \qquad \text{eq. 2}$$

where P_{em} is emission intensity, P_{ex} is excitation intensity, n is the number of photons involved in the process and A is constant. There are various two-photon processes, such as energy transfer upconversion (efficiency $\eta = 10^{-3}$), excited state absorption ($\eta = 10^{-5}$), cooperative sensitization ($\eta = 10^{-6}$), cooperative luminescence ($\eta = 10^{-8}$), second

Doi:10.1016/j.jlumin.2012.12.033

harmonic generation ($\eta = 10^{-11}$) and two-photon absorption excitation ($\eta = 10^{-13}$).[1] The efficiency of energy transfer upconversion, which occurs in Y_2O_3:Er,Yb, is higher than that of the other two-photon processes. Logarithmic transformation of both sides of eq. 2 is gives the following:

$$\log P_{em} = n \log P_{em} + C \qquad \text{eq. 3}$$

where C is a constant. The slope of the double logarithmic plot is the number of photons involved in the process. A double logarithmic plot at an average particle size of 22 nm is shown in Figure 7. The number of photons involved in the process at each particle size is summarized in Table 1. The number of photons involved in the process of green emission is approximately 2.6, and that of red emission is approximately 2.3. The number of photons involved in the process of bulk Y_2O_3:Er,Yb is usually two because luminescence is generated through a two-photon process[63] as shown in Figure 6. The number of photons involved in the process of Y_2O_3:Er,Yb nanoparticles is slightly larger than that of bulk Y_2O_3:Er,Yb. Three-photon process may occur to some degree. Therefore, the observed number of photon increased slightly, reaching a value between two and three. The following are conceivable three-photon processes. Green emission features two nonradiative relaxations, as shown in Figure 8(a).

$^4I_{15/2} \rightarrow {}^4I_{11/2}$

$^4I_{11/2} \rightarrow {}^4I_{13/2}$ (nonradiative relaxation)

Doi:10.1016/j.jlumin.2012.12.033

$^4I_{13/2} \rightarrow {}^4F_{9/2}$

$^4F_{9/2} \rightarrow {}^2H_{9/2}$

$^2H_{9/2} \rightarrow {}^2H_{11/2}/{}^4S_{3/2}$ (nonradiative relaxation)

$^2H_{11/2}/{}^4S_{3/2} \rightarrow {}^4I_{15/2}$

Red emission features one nonradiative relaxation, as shown in Figure 8(b).

$^4I_{15/2} \rightarrow {}^4I_{11/2}$

$^4I_{11/2} \rightarrow {}^4I_{13/2}$ (nonradiative relaxation)

$^4I_{13/2} \rightarrow {}^4F_{9/2}$

$^4F_{9/2} \rightarrow {}^2H_{9/2}$

$^2H_{9/2} + {}^4I_{13/2} \rightarrow {}^4F_{9/2} + {}^4F_{9/2}$ (cross relaxation)

$^4F_{9/2} \rightarrow {}^4I_{15/2}$

The three-photon mechanism ($^4I_{13/2} \rightarrow {}^4F_{9/2}$, $^4F_{9/2} \underline{\rightarrow} {}^2H_{9/2}$) can occur by Er^{3+} excitation and energy transfer from two Yb^{3+} ions.[1] Both green and red emission processes involve nonradiative relaxation. As mentioned above, the specific surface area increases significantly as the particles approach the nanoscale, causing an enhancement in nonradiative relaxation. Therefore, the number of photons involved in the process of the nanoparticles increased because the three-photon process was accelerated by the increase in nonradiative relaxation.

Doi:10.1016/j.jlumin.2012.12.033

4. Conclusions

We fabricated Y_2O_3:Er,Yb upconversion nanoparticles by laser ablation in water. Strong red luminescence was observed by upconversion spectroscopy. The energy transfer from nanoparticles to water molecules accelerated the observed nonradiative relaxation and led to an intense red emission, which featured nonradiative relaxation. Another important observation was the increase in the number of photons involved in the process of the upconversion nanoparticles, which was the result of a mixture of two-photon and three-photon processes, while the number of photons involved in the process of Y_2O_3:Er,Yb bulk was the result of a two-photon process. This finding was also attributed to the increase in nonradiative relaxation, which occurred through the three-photon process of the Y_2O_3:Er,Yb nanoparticles.

Acknowledgements

The authors wish to thank K. Nakamura (Laser ablation), H. Iida and Y. Suzuki (XRD) of Tokyo Tech. This study was supported by JSPS KAKENHI Grant and the Collaborative Research Project of Materials & Structures Laboratory.

References

1 F. Auzel., Chem. Rev. 104 (2004) 139-173.

2 F. Auzel and F. C. R. Acad. Sci. (Paris), 262 (1966) 1016.

3 F. Auzel and F. C. R. Acad. Sci. (Paris), 263B (1966) 819.

4 V. Ovsyankin and P. P. Feofilov, Jetp Lett. 3 (1966) 317.

5 V. Ovsyankin and P. P. Feofilov, Jetp Lett. 3 (1966) 322.

6 M. Pollnau, D. R. Gamelin, S. R. Luthi and H. U. Gudel, Phys. Rev. B, 2000, 61, 3337-3346.G.

7 H. Dieke and H. M. Crosswhite, Appl. Opt. 2 (1963) 675-686.

8 S. Heer, K. Kompe, H. U. Gudel and M. Haase, Adv. Mater. 16 (2004) 2102-2105.

9 M. Kamimura, D. Miyamoto, Y. Saito, K. Soga and Y. Nagasaki, Langmuir, 24 (2008) 8864-8870.

10 A. Shalav, B. S. Richards, T. Trupke, K. W. Krämer and H. U. Güdel, Appl. Phys. Lett. 86 (2005) 013505.

11 J. Zhou, Z. Liu and F. Li, Chem. Soc. Rev. 41 (2012) 1323-1349.

12 R. Weissleder, Nature Biotechnology, 19 (2001) 316-317.

13 M. Wang, C. C. Mi, Y. X. Zhang, J. L. Liu, F. Li, C. B. Mao and S. K. Xu, J. Phys. Chem. C, 113 (2009) 19021-19027.

14 R. Kumar, M. Nyk, T. Y. Ohulchanskyy, C. A. Flask and P. N. Prasad, Adv. Funct. Mater.

19 (2009) 853-859.

15 M. Wang, C. C. Mi,W. X.Wang, C. H. Liu, Y. F. Wu, Z. R. Xu, C. B. Mao and S. K. Xu, ACS Nano, 3 (2009) 1580-1586.

16 Q. Q. Zhan, J. Qian, H. J. Liang, G. Somesfalean, D. Wang, S. L. He, Z. G. Zhang and S. Andersson-Engels, ACS Nano, 5 (2011) 3744-3757.

17 L. Q. Xiong, Z. G. Chen, Q. W. Tian, T. Y. Cao, C. J. Xu and F. Y. Li, Anal. Chem. 81 (2009) 8687-8694.

18 Q. Liu, Y. Sun, C. G. Li, J. Zhou, C. Y. Li, T. S. Yang, X. Z. Zhang, T. Yi, D. M. Wu and F. Y. Li, ACS Nano, 5 (2011) 3146-3157.

19 L. Cheng, K. Yang, S. Zhang, M. W. Shao, S. T. Lee and Z. Liu, Nano Res. 3 (2010) 722-732.

20 S. A. Hilderbrand, F. W. Shao, C. Salthouse, U. Mahmood and R. Weissleder, Chem. Commun. 2009 (2009) 4188-4190.

21 P. Zhang, W. Steelant, M. Kumar and M. Scholfield, J. Am. Chem. Soc. 129 (2007) 4526-4527.

22 Y. Y. Guo, M. Kumar and P. Zhang, Chem. Mater. 19 (2007) 6071-6072.

23 H. S. Qian, H. C. Guo, P. C. L. Ho, R. Mahendran and Y. Zhang, Small, 5 (2009) 2285-2290.

24 J. N. Shan, S. J. Budijono, G. H. Hu, N. Yao, Y. B. Kang, Y. G. Ju and R. K. Prud'homme, Adv. Funct. Mater. 21 (2011) 2488-2495.

25 C. Wang, H. Q. Tao, L. Cheng and Z. Liu, Biomaterials, 32 (2011) 6145-6154.

26 M. S. Patterson, B. C. Wilson and D. R. Wyman, Lasers Med. Sci. 6 (1991) 379-390.

27 J. R. Darwent and G. Porter, Chem. Commun. 1981 (1981) 145-146.

28 E. O. Knutson and K. T. Whitby, J. Aerosol Sci. 6 (1975) 443-451.

29 R. G. Osifchin, W. J. Mahoney, J. D. Bielefeld, R. P. Andres, J. I. Henderson and C. P. Kubiak, Superlattices and Microstructures, 18 (1995) 283-289.

30 J. Neddersen, G. Chumanov and T. Cotton, Appl. Spectroscopy, 47 (1993) 1959-1964.

31 A. Fojtik and A. Henglein, Ber. Bunsen. Phys. chem. 97 (1993) 252-254.

32 F. Mafune, J. Y. Kohno, Y. Takeda, T. Kondow and H. Sawabe, J Phys. Chem. B, 104 (2000) 8333-8630.

33 C. L. Sajti, R. Sattari, B. N. Chichkov and S. Barcikowski, J. Phys. Chem. C, 114 (2010) 2421.

34 H. Zeng, W. Cai, Y. Li, J. Hu and P. Liu, J. Phys. Chem. B, 109 (2005) 18260-18266.

35 M. A. Gondal, Q. A. Drmosh, Z. H. Yamani and T. A. Saleh, Appl. Surf. Sci. 256 (2009) 298-304.

36 D. Tan, Y. Teng, Y. Liu, Y. Zhuang and J. Qiu, Chem. Lett. 38 (2009) 1102-1103.

37 S. Z. Khan, Y. Yuan, A. Abdolvand, M. Schmidt, P. Crouse, L. Li, Z. Liu, M. Sharp and K. G. Watkins, J. Nanopart. Res. 11 (2009) 1421-1427.

38 K. Y. Niu, J. Yang, S. A. Kulinich, J. Sun and X. W. Du, Langmuir, 2010, 26, 16652-16657.

39 X. Z. Lin, P. Liu, J. M. Yu and G. W. Yang, J. Phys. Chem. C, 113 (2009) 17543-17547.

40 H. Zhang, C. Liang, Z. Tian, G. Wang and W. Cai, J. Phys. Chem. C, 114 (2010) 12524-12528.

41 S. Z. Khan, Z. Liu and L. Li, Appl. Phys. A, 101 (2010) 781-787.

42 P. Liu, W. Cai, M. Fang, Z. Li, H. Zeng, J. Hu, X. Luo and W. Jing, Nanotechnology, 20 (2009) 285707.

43 H. Usui, Y. Shimizu, T. Sasaki and N. Koshizaki, J. Phys. Chem. B, 109 (2005) 120–124.

44 G. S. Park, K. M. Kim, S. W. Mhin, J. W. Eun, K. B. Shim, J. H. Ryu, N. Koshizaki, Electrochem. Solid-State Lett. 11 (2008) J23-J26.

45 D. Katsuki, T. Sato, R. Suzuki, Y. Nanai, S. Kimura and T. Okuno, Appl. Phys. A, 108 (2012) 321-327.

46 F. Yoshimura, K. Nakamura, F. Wakai, M. Hara, M. Yoshimoto, O. Odawara and H Wada, Appl. Surf. Sci. 257 (2011) 2170-2175.

47 B. Y. Kokuoz, K. Serivalsatit, B. Kokuoz, O. Geiculescu, E. McCormick and J. Ballato, J. Am. Ceram. Soc. 92 (2009) 2247-2253.

48 F. Vetrone, J. C. Boyer, J. A. Capobianco, A. Speghini and M. Bettinelli, J. Mater. Res. 19 (2004) 3398-3407.

49 S. Chandra, F. L. Deepak, J. B. Gruber and D. K. Sardar, J. Phys. Chem. C, 114 (2010) 874-880.

50 N. Venkatachalam, Y. Saito and K. Soga, J. Am. Ceram. Soc. 92 (2009) 1006-1010.

51 G. De, W. Qin, J. Zhang, J. Zhang, Y. Wang, C. Cao and Y. Cui, J. Lumin. 119-120 (2006) 258-263.

52 H. Eilers, J. Alloys Comp. 474 (2009) 569-572.

53 T. Nunokawa, Y. Onodera, M. Hara, Y. Kitamoto, O. Odawara and H. Wada, Appl. Surf. Sci. 261 (2012) 118-122.

54 S. Kaniya and H. Mizuno, “Phosphors for lamps,” in: W. M. Yen, S. Shionoya and H. Yamamoto (Eds.), Phosphor Handbook, CRC Press, Boca Raton, FL. 2006, Chapter 5.6.

55 T. Kano, “Luminescence centers of rare-earth ions,” in: W. M. Yen, S. Shionoya and H. Yamamoto (Eds.), Phosphor Handbook, CRC Press, Boca Raton, FL. 2006, Chapter 3.3.

56 Y. Haas and G. Stein, Chem. Phys. Lett. 15 (1972) 12-16.

57 W. Siebrand, J. Chem. Phys. 46 (1967) 440-447.

58 L. A. Riseberg and H. W. Moos, Phys. Rev. 174 (1968) 429-438.

59 S. Suzer and L. Andrews, Chem. Phys. Lett. 140 (1987) 300-305.

60 H. Yada, M. Nagai and K. Tanaka, Chem. Phys. Lett. 473 (2009) 279-283.

61 C. P. Lawrence and J. L. Skinner, J. Chem. Phys. 118 (2003) 264-272.

62 F. Song, G. Zhang, M. Shang, H. Tan, J. Yang, and F. Meng, Appl. Phys. Lett. 79 (2001) 1748-1750.

63 Y. Lu and N. Ming, J. Mater. Sci. 30 (1995) 5705.

Figure captions

Figure 1. XRD pattern of target (a) and nanoparticles (b).

Figure 2. SEM image of nanoparticles.

Figure 3. Nanoparticle size distribution.

Figure 4. Average particle size as a function of irradiating laser energy at target.

Figure 5. Upconversion spectra of nanoparticles (λ_{ex}: 980 nm).

Figure 6. Two-photon processes in energy diagram of Er^{3+} ion: (a) green emission and (b) red emission.

Figure 7. Double logarithmic plot of emission intensity as a function of excitation intensity.

Figure 8. Three-photon processes in an energy diagram of an Er^{3+} ion: (a) green emission and (b) red emission.

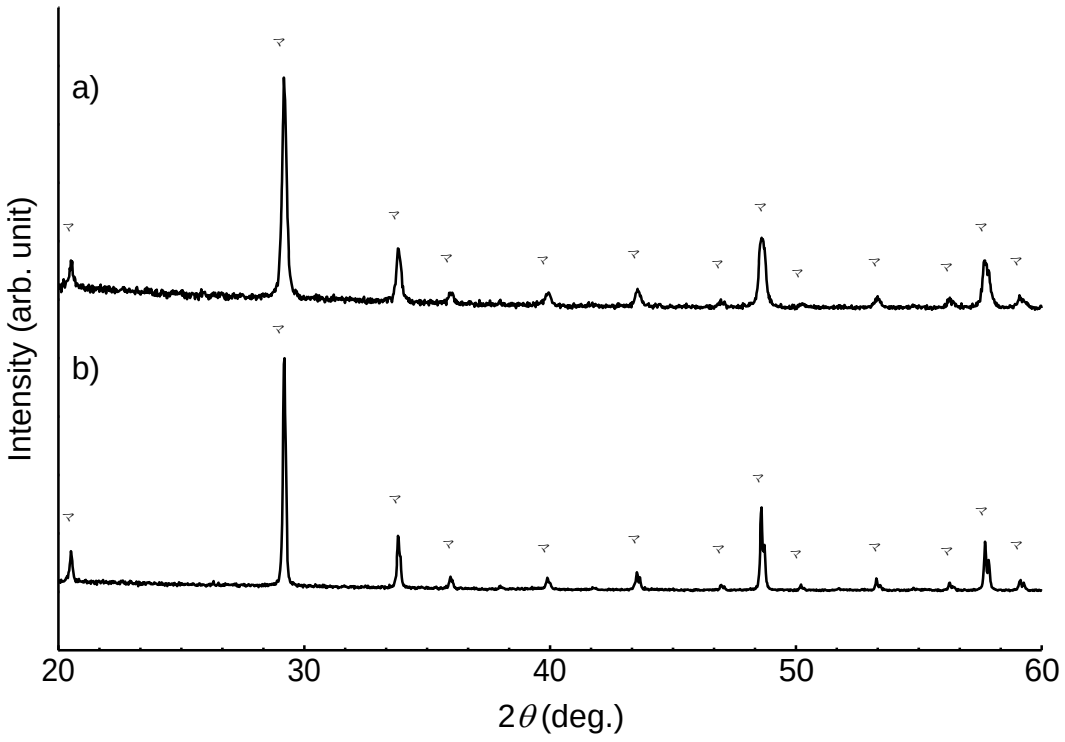

Figure 1. XRD pattern of target (a) and nanoparticles (b).

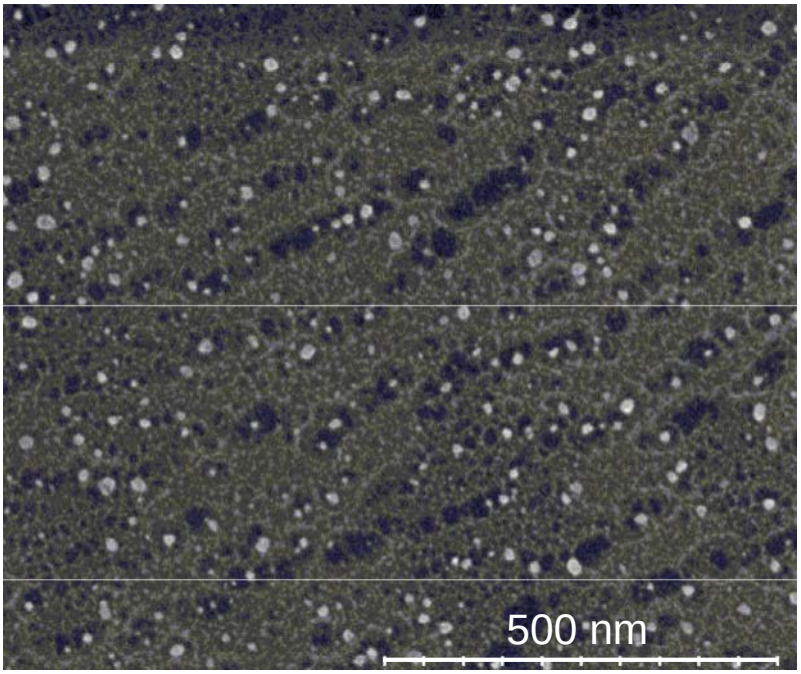

Figure 2. SEM image of nanoparticles.

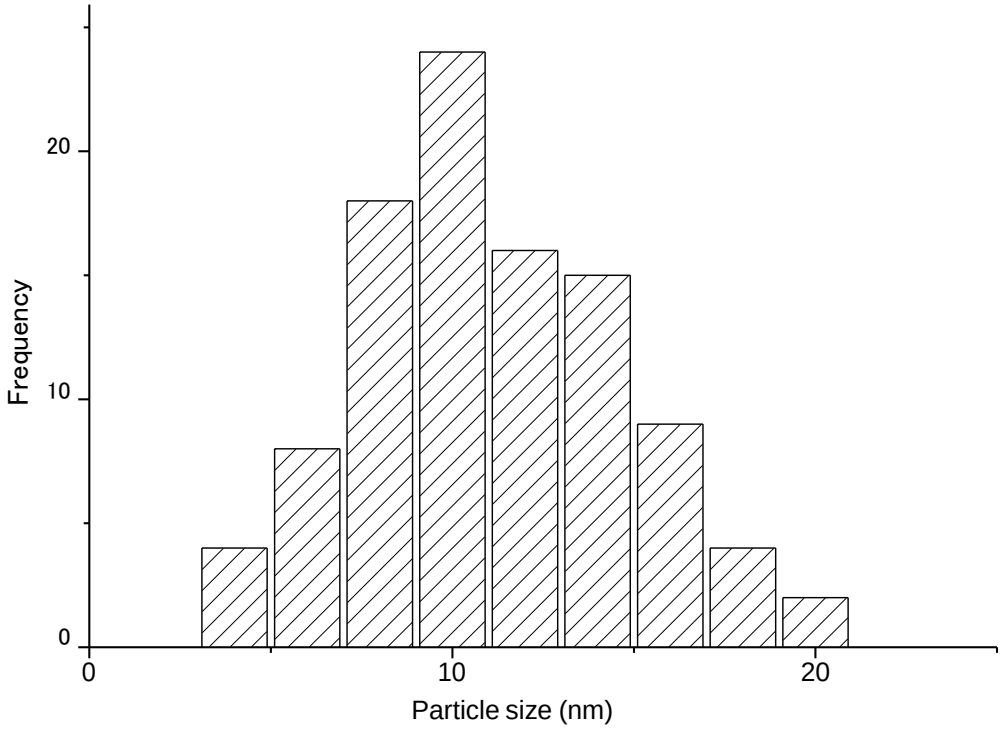

Figure 3. Nanoparticle size distribution.

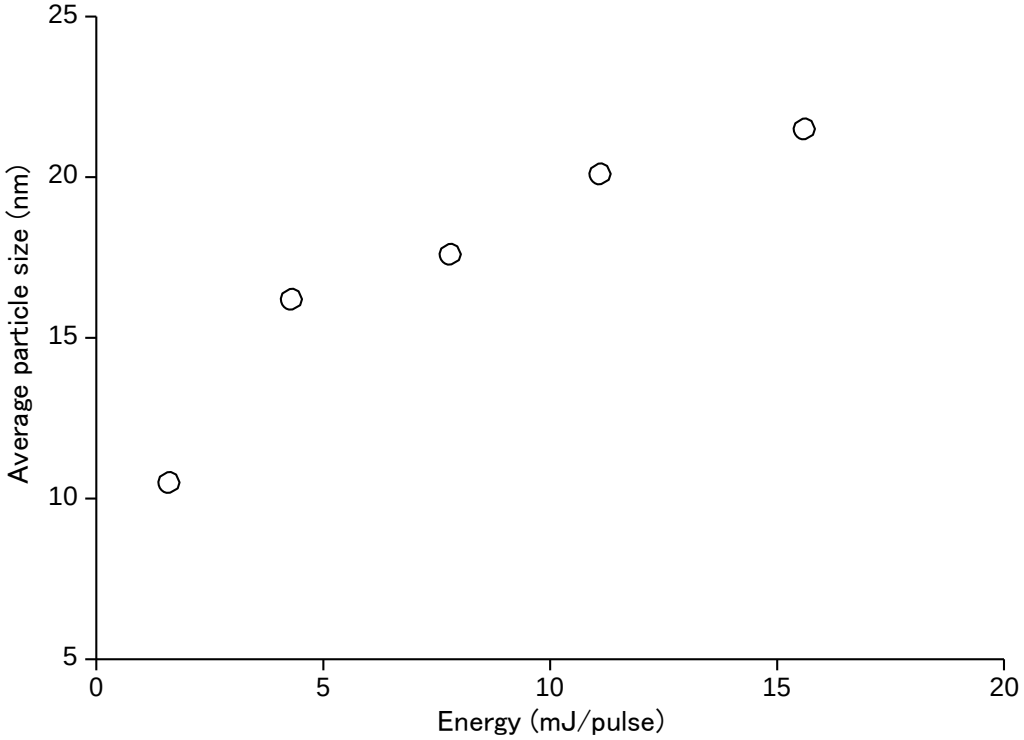

Figure 4. Average particle size as a function of irradiating laser energy at target.

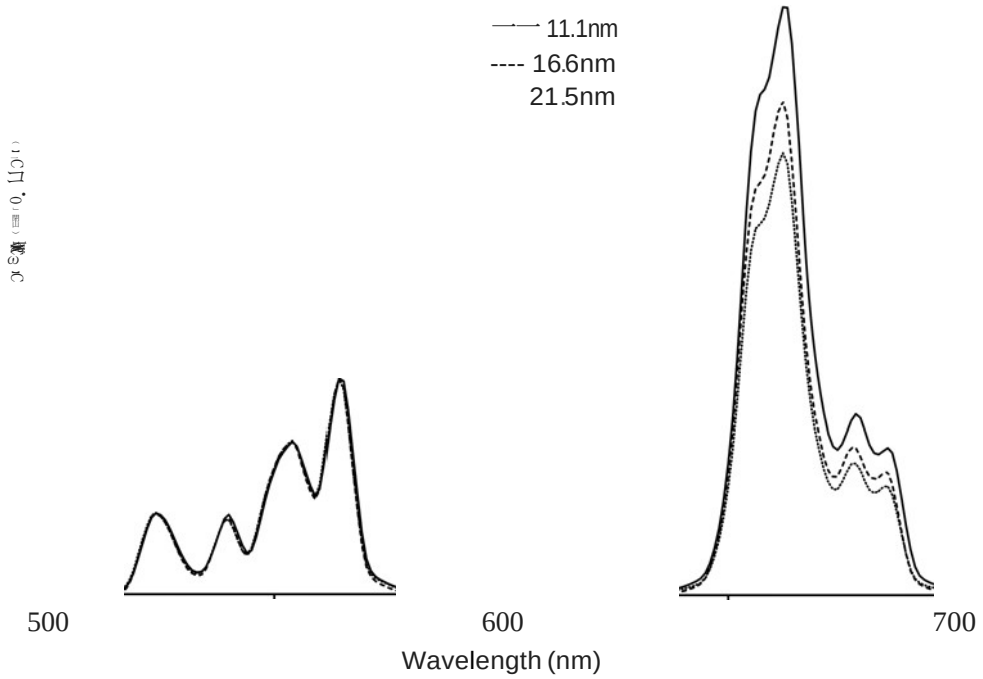

Figure 5. Upconversion spectra of nanoparticles (excitation wavelength: 980 nm).

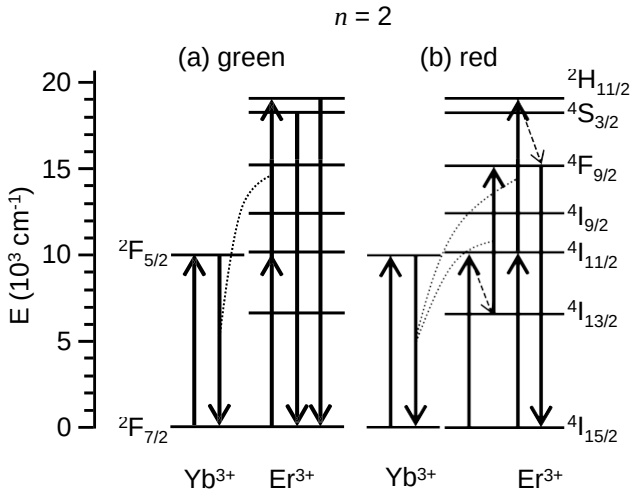

Figure 6. Two-photon processes in energy diagram of Er^{3+} ion: (a) green emission and (b) red emission.

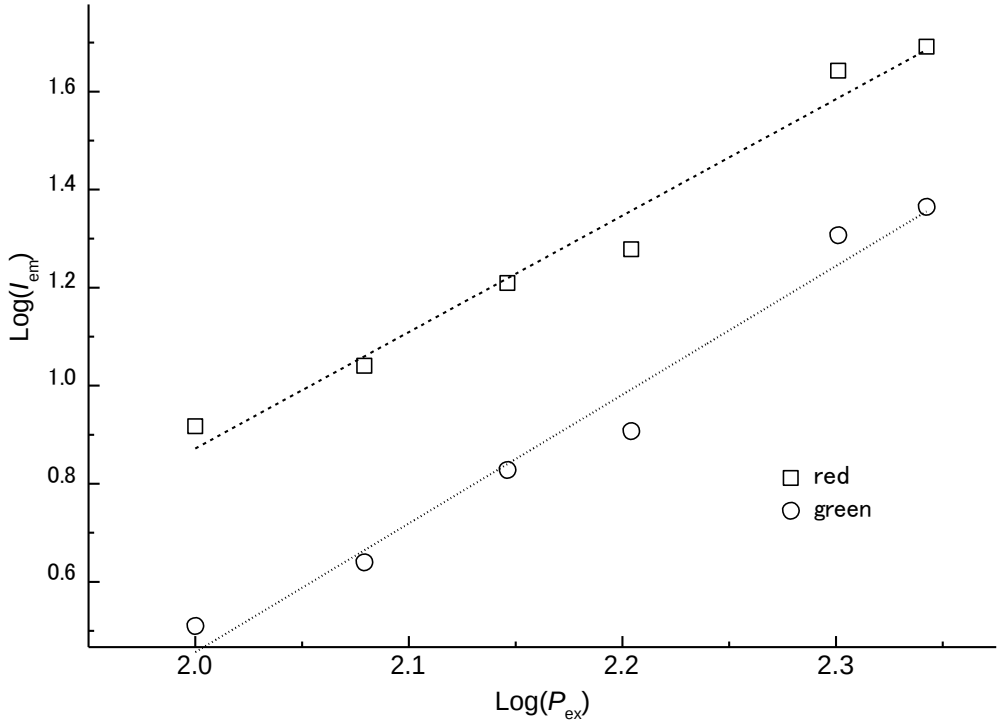

Figure 7. Double logarithmic plot of emission intensity as a function of excitation intensity.

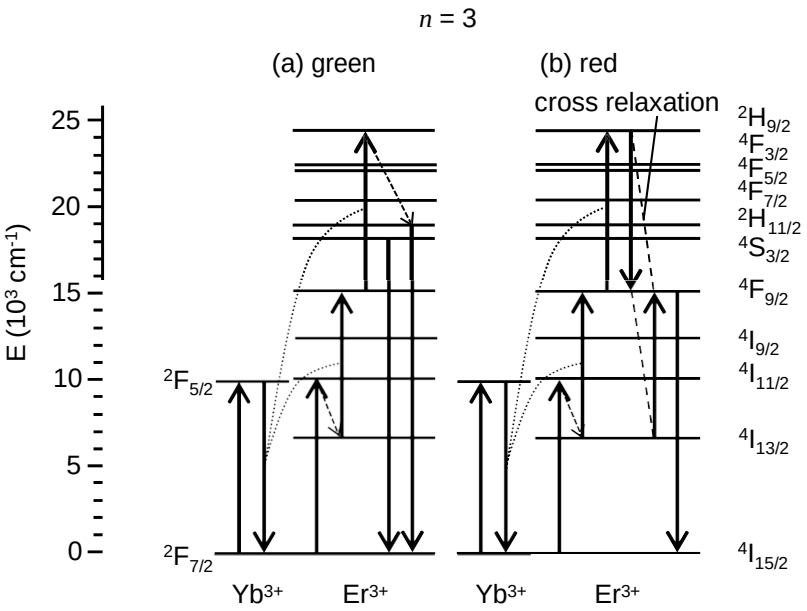

Figure 8. Three-photon processes in an energy diagram of an Er^{3+} ion: (a) green emission and (b) red emission.